Fluorescent Polymer-AS1411-Aptamer Probe for dSTORM Super-Resolution Imaging of Endogenous Nucleolin

Laura Fabre, Corentin Rousset, Karine Monier, Fernande da Cruz-Boisson, Philippe Bouvet, Marie-Thérèse Charreyre, Thierry Delair, Etienne Fleury, Arnaud Favier

Fluorescent polymer-AS1411-aptamer probe for dSTORM super-resolution imaging of endogenous nucleolin

Laura Fabre,[1] Corentin Rousset,[2†] Karine Monier,[2†] Fernande Da Cruz-Boisson,[1] Philippe Bouvet,[2] Marie-Thérèse Charreyre,[1] Thierry Delair,[1] Etienne Fleury,[1] Arnaud Favier[1]*

[1]*Univ Lyon, Université Lyon1, INSA Lyon, UMR CNRS 5223, Ingénierie des Matériaux Polymères, Villeurbanne, F-69622, France.*

[2]*Univ Lyon, Centre Léon Bérard, UMR INSERM 1052 CNRS 5286, Centre de recherche en cancérologie de Lyon, Lyon, F-69008, France.*

[†]*Present address: Univ Lyon 1, CNRS UMR 5310 - INSERM U1217, Institut NeuroMyoGene, Lyon, F-69008, France*.

ABSTRACT

Nucleolin is a multifunctional protein involved in essential biological processes. To precisely localize it and unravel its different roles in cells, fluorescence imaging is a powerful tool, especially super-resolution techniques. Here, we developed polymer-aptamer probes, both small and bright, adapted to dSTORM nanoscopy. Well-defined fluorescent polymer chains bearing fluorophores (AlexaFluor647) and a reactive end-group were prepared via RAFT polymerization. The reactive end-group was then used for the oriented conjugation with AS1411, a DNA aptamer that recognizes nucleolin with high affinity. Conjugation via strained alkyne/azide click chemistry (SPAAC) between dibenzylcyclooctyne (DBCO)-ended fluorescent polymer chains and 3'-azido-functionalized nucleic acids proved to be the most efficient approach. *In vitro* and *in cellulo* evaluations demonstrated that selective recognition for nucleolin was retained. Their brightness and small size make these polymer-aptamer probes an appealing alternative to immunofluorescence, especially for super-resolution (10-20 nm) nanoscopy. dSTORM imaging demonstrated the ability of our fluorescent polymer-aptamer probe to provide selective and super-resolved detection of cell surface nucleolin.

KEYWORDS. Fluorescent polymer probes, Polymer-aptamer conjugation, AS1411 aptamer / nucleolin recognition, Strain-promoted azide-alkyne click chemistry (SPAAC), Protein labeling, dSTORM super-resolution fluorescence nanoscopy.

INTRODUCTION

Nucleolin (NCL) is a multifunctional protein found at several locations inside cells.[1] As the name suggests, it is very abundant in the nucleolus within the nucleus. However, it is also found in the cytoplasm and at the plasma membrane. Although NCL has been discovered several decades ago, its functions inside cells have only been partially investigated. Previous studies have revealed that this protein is involved in several biological processes such as cell survival and proliferation,[2] but also related to cardiovascular and neurological diseases, inflammation, cancer, bacterial and viral infections.[2-6] Nucleolin has been found over-expressed at the surface of cancer cells compared to healthy ones, notably in the case of pancreatic cancer that exhibits one of the poorest survival rate (5% after 5 years).[7-11] Furthermore, cell surface NCL is involved in the anchoring of human immunodeficiency virus type 1 (HIV-1) to its target cells.[12]

Precisely locating NCL is thus crucial to study its regulation and functions. One of the main techniques to achieve this goal is fluorescence imaging, including live cell videomicroscopy and confocal microscopy (>200 nm resolution). Furthermore, super-resolution techniques such as direct stochastic optical reconstruction microscopy (dSTORM) now enable to reach 5-30 nm resolution.[13] dSTORM imaging is based on the use of organic dyes (like AlexaFluor 647, AF647)[14] that reversibly enter a dark/bright cycle (blinking) thanks to adequate buffer and light irradiation. The resulting stochastic fluorescence emission then enables to spot the individual emitters with a very high localization precision and to reconstruct point-by-point super-resolved images.[15]

Fluorescence labeling of endogenous cellular NCL is commonly achieved by immunofluorescence.[1] Two different approaches are possible: a direct approach relies on fluorescent primary antibodies exhibiting a highly specific recognition for NCL. However, they

are difficult to label and often exhibit a moderate brightness. Therefore, a two-step indirect approach is generally preferred, using unlabeled primary antibodies then labeled with fluorescent secondary antibodies. Although efficient, this indirect approach is tedious and may not be suitable for some studies like the detection of cell surface proteins, especially those being rapidly internalized. Moreover, it is noteworthy that, due to the high molecular weight of antibodies (≈150 000 $g.mol^{-1}$ for IgGs), such primary-secondary antibody sandwich may reach up to 20 nm in size, what becomes an issue for super-resolution imaging as the size of the labeling system falls in the same order than localization precision.

An attractive alternative to antibodies is aptamers since they are smaller in size and show high specificity for their target protein. AS1411 is a 26-base guanine-rich DNA aptamer (5'-GGT-GGT-GGT-GGT-TGT-GGT-GGT-GGT-GGT-3', 7 800 $g.mol^{-1}$) exhibiting a G-quadruplex 3D conformation that binds with a high affinity ($K_d \approx 10^{-9}$ - 10^{-12} M) to a nucleic acid binding domain of endogenous NCL.[6, 9, 16-17] AS1411 has been shown to exert an anti-proliferative activity against various cancer cell lines[9] and is able to inhibit HIV-1 target cell infection.[12] Fluorescent AS1411 aptamers, generally labeled at their 3' or 5' chain-end during synthesis or through conjugation with a reactive dye, have been used to label NCL *in cellulo*.[18] However, aptamers labeled with only one fluorophore may lack brightness. Alternatively, AS1411 has been immobilized at the surface of various kinds of bright fluorescent particles, either organic or inorganic.[9, 19] However, in this case, several aptamers are generally immobilized and each particle may bind several NCL at the same time. In addition, due to the overall size of such system, this strategy is not adapted to super-resolution nanoscopy. The challenge is thus to modify AS1411 aptamer with bright fluorescent labels compatible with super-resolution imaging, while retaining overall a small size and a high recognition for the target protein, nucleolin.

In our group, we have developed well-defined fluorescent polymer probes that combine hydrophilic copolymer chains (synthesized by RAFT polymerization) and a controlled number of organic dyes covalently bound along the chain (Figure 1A). These modular probes are highly water-soluble, biocompatible and can be labeled with various types of chromophores.[20-21] In addition, brightness and resistance to photobleaching are enhanced compared to the corresponding molecular dyes.[21] Moreover, this tunable platform can be functionalized in a controlled manner with different reacting groups or biospecific ligands. Indeed, we have already shown that such fluorescent polymer chains can be end-functionalized for an oriented conjugation onto native or recombinant proteins.[22-24] Finally, the size of these fluorescent polymer probes remains small, generally below 10 nm, and is controlled by the molecular weight of the polymer chain that can be adjusted thanks to the RAFT polymerization process.[25] Such fluorescent polymer probes are thus attractive candidates to tag AS1411 aptamer in order to precisely localize NCL by fluorescence imaging.

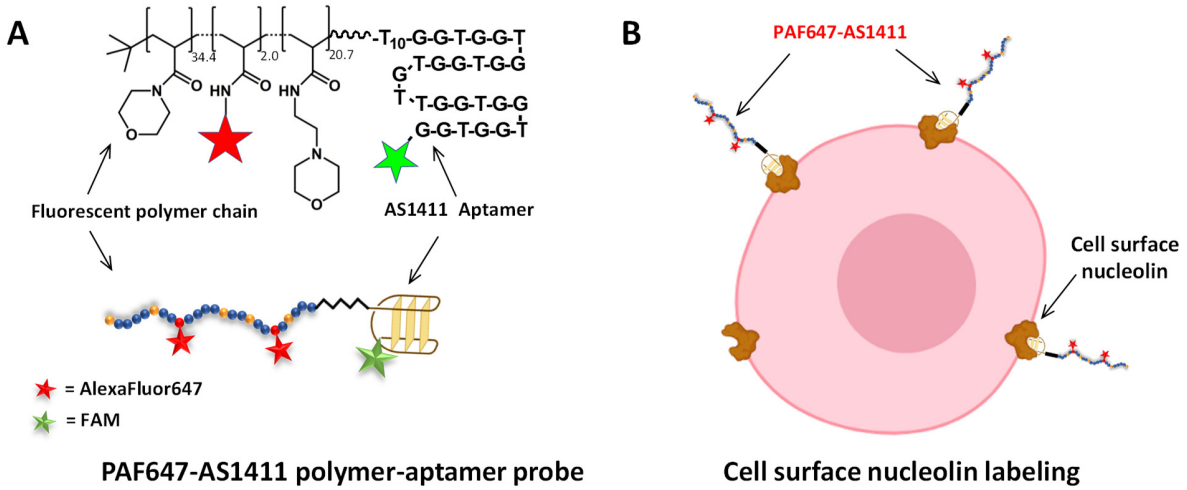

Figure 1. Chemical structure and schematic representation of the fluorescent polymer-aptamer probe (A) and illustration of the labeling of endogenous nucleolin at the cell membrane (B).

The objective of this work was thus to develop an approach to conjugate our fluorescent polymer chains (labeled with AF647 fluorophores for imaging) to AS1411 aptamer. In order for the aptamer to maintain its G-quadruplex folding and NCL recognition properties, we opted for an oriented conjugation between one chain-end of both the aptamer (tagged with a FAM dye for sake of characterization) and the polymer (Figure 1A). Literature is quite abundant on the conjugation of nucleic acids in lateral position of polymer chains, however examples of such oriented conjugation at the chain-end are scarcer.[26-32] Conjugation can be performed by "grafting from",[27] but it often relies on "grafting onto" approaches consisting in the separate preparation of the polymer and the aptamer before conjugation. Oriented chain-end conjugation has been performed mainly with PEG derivatives and homopolymers.[33-36] Generally, conjugation is achieved via thiol-maleimide,[33] activated ester/amine[32, 34] or more recently using azide-alkyne coupling chemistries[35-37]. In this study, two different polymer-aptamer conjugation strategies were compared, either the activated ester/primary amine coupling or the more recent bio-orthogonal strain-promoted azide/alkyne click chemistry (SPAAC). The latter has indeed shown to be very efficient without the use of potentially cytotoxic copper catalysts.[38] To further preserve the aptamer conformation, a nucleotidic sequence of 10 thymines (T_{10}) was added at the AS1411 chain-end. The introduction of an extra oligoethylene glycol spacer on the aptamer was also explored.

The polymer chain was functionalized with AF647 fluorophores for microscopy studies, before modification of one of its chain-end to introduce a reactive group for aptamer coupling. After conjugation, we evaluated if the aptamer retained its specificity for NCL recognition. Then, the polymer-aptamer probe was used to visualize *in cellulo* endogenous NCL (Figure 1B) in several fluorescence microscopy studies. This strategy was compared to immunofluorescence. Finally, NCL was precisely localized at the cell surface by dSTORM super-resolution nanoscopy.

EXPERIMENTAL SECTION

Materials. *N*,*N*-diisopropylethylamine (DIPEA, Sigma-Aldrich, ≥99,5%), triethylamine (TEA, Aldrich, 95%), dimethylphenylphosphine (DMPP, Aldrich, 99%), *4*-(*2*-aminoethyl)morpholine (AEM, Aldrich, 99%), dibenzylcyclooctyne-amine (DBCO-NH_2, Jena Bioscience, >95% (RMN)), AlexaFluor647 cadaverine (AF647-NH_2, Invitrogen), anhydrous *N*,*N*-dimethylformamide (DMF, Acros, 99.8%), chloroform ($CHCl_3$, Fisher), anhydrous dimethylsulfoxide (DMSO, Acros, 99.7%), diethyl ether (Et_2O, Sigma-Aldrich, ≥99.5%), methanol (MeOH, Merck, 99.8%), phosphate buffered saline (PBS pH 7.4, Gibco), sterile water (Otec, Aguettant), ultrapure distilled water (Invitrogen), 40% acrylamide/bis-acrylamide 37.5 :1 (Bio-rad), Tween 20 (Sigma Aldrich), tetramethylethylenediamine (TEMED, Sigma) were used as received.

Aptamers and Crich DNA sequences (shown below) were supplied by Eurogentech and Integrated DNA Technologies (IDT) after purification by RP-HPLC (Table S1): FAM-AS1411-N_3 (IDT, 80%, 5'-*6*-FAM; 3'-N_3), FAM-AS1411-PEG-N_3 (IDT, 85%, 5'-*6*-FAM; 3'-PEG_3-N_3), FAM-AS1411-NH_2 (Eurogentec, 5'-*6*-FAM; 3'-NH_2), AS1411-NH_2 (Eurogentec, 3'-NH_2), FAM-Crich-N_3 (IDT, 96%, 5'-*6*-FAM; 3'-N_3).

AS1411 sequence: (5'-GGT-GGT-GGT-GGT-TGT-GGT-GGT-GGT-GGT-TTT-TTT-TTT-3')

Crich sequence: (5'-CCT-CCT-CCT-CCT-TCT-CCT-CCT-CCT-CCT-TTT-TTT-TTT-3')

Methods.

^1H NMR. Spectra were recorded in the indicated deuterated solvent at room temperature (298 K) on a Bruker Avance III spectrometer operating at 400.1 MHz for ^1H observation with a 5mm BBFO+ probe.

SEC-MALLS. Size exclusion chromatography coupled with multi-angle laser light scattering (SEC/MALLS) was performed using a set-up composed of a Shimadzu LC-6A liquid chromatography pump (1 mL.min^{-1}) and a PLgel Mixed-C column (5µm pore size). Online double detection was composed of a differential refractometer (Waters DRI 410) and a three-angle (46°, 90°, 133°) MiniDAWN TREOS light scattering detector (Wyatt Technologies), operating at 658 nm. Analyses were performed by injection of 70 µL of polymer solution (3 mg.mL^{-1}) in chloroform. The specific refractive index increment (dn/dc) for the polymers in the same eluent (0.130 mL.g^{-1}) was previously determined with a NFT ScanRef monocolor interferometer operating at 633 nm. The average molar mass and dispersity data were determined using the Wyatt ASTRA software package.

RAFT polymerization. Poly(*N*-acryloylmorpholine) homopolymer (PNAM-DB, M_n = 10 300 g.mol^{-1}, DP_n = 71, $Đ$ = 1.1) and Poly(*N*-acryloylmorpholine-*stat*-*N*-acryloxysuccinimide) copolymer (P(NAM-*stat*-NAS)-DB, M_n = 8 900 g.mol^{-1} , DP_n = 57, $Đ$ = 1.1), both with α-tert-butyl (^{t}Bu) and ω-dithiobenzoate (DB) chain-ends were synthesized by RAFT polymerization following previously reported procedures (see details in supporting information (SI) and Figure S1).[25,39] The purified polymers were characterized by SEC-MALLS and ^{1}H NMR (Figure S2). SEC-MALLS showed monomodal and narrow molecular weight distributions. Experimental molecular weight determined by SEC-MALLS and ^{1}H NMR were in close agreement with the predicted ones indicating a good control over the polymerization.

Synthesis of polymer chain with a DBCO ω-chain-end. PAF647-NHS ester was synthetized as described in a previous article[22] from the P(NAM-*stat*-NAS)-DB reactive copolymer precursor (see details in SI). An average of 2.0 AF647-NH_2 fluorophores (Invitrogen) was coupled along the

chain before capping of the remaining reactive units with aminoethylmorpholine (AEM). AF647 coupling yield (96%) was determined by SEC-UV at 647 nm (Figure S3) following the published procedure.[20]

PAF647-DBCO was then synthesized by reacting a 146 µL anhydrous DMF solution containing PAF647-NHS ester (10.0 mg, 0.9 µmol, M_n = 11 100 g.mol^{-1}, N_f = 2.0, 1 eq.) and DIPEA (1.7 µL, 10.0 µmol) with a 187 µL anhydrous DMF solution of DBCO-NH_2 (5.6 mg, 4.5 µmol, 5.0 eq.). The blue solution (30 g.L^{-1} polymer concentration) was stirred at room temperature for 4h under argon. PAF647-DBCO polymer was then purified at 4°C by 3 consecutive precipitations in a large volume of diethyl ether/chloroform 2/1 v/v with re-solubilization in methanol/triethylamine 60/1 v/v to ensure a good recovery of the polymer and elimination of the residual DMF from the polymer sample. Finally, the blue PAF647-DBCO polymer was dried under vacuum (4.5 mg, 0.4 µmol, N_f = 2.0, M_n = 11 300 g.mol^{-1}).

Reference AEM-capped copolymers (CPAEM) were prepared from the same P(NAM-*stat*-NAS)-DB reactive copolymer precursor than their PAF647 counterparts but without the addition of AF647 fluorophores. PNAM-DBCO (M_n = 10 600 g.mol^{-1}, DP_n = 71) (Figure S4) and CPAEM-DBCO (M_n = 9 300 g.mol^{-1}, DP_n = 57) were synthetized using the same procedure than PAF647-DBCO, except than anhydrous DMF was replaced by $CHCl_3$ as the solvent.

Polymer-aptamer conjugation.

Aptamer conjugation with polymers bearing an NHS ester ω-chain end. Typically, the aptamer FAM-AS1411-NH_2 (5'-FAM-GGT-GGT-GGT-GGT-TGT-GGT-GGT-GGT-GGT-TTT-TTT-TTT-NH_2-3') (133.0 µg, 11.0 nmol, M = 12 061.1 g.mol^{-1}, 1 eq.) was solubilized in 20.7 µL of

sterile aqueous buffer (pH 7.4 PBS with 1M NaCl) before addition of a 20.7 µL solution of PAF647-NHS ester polymer (1.3 mg, 118.0 nmol, M_n = 11 100 g.mol^{-1}, 10 eq.) in anhydrous DMSO containing 0.7% of DIPEA (4eq.). The blue solution was stirred in a thermomixer (800 rpm) at 37°C for 24h. The raw product (Table S2) was characterized by gel electrophoresis in native conditions (Figure S5).

Aptamer conjugation with polymers bearing a DBCO ω-chain end. Typically, the aptamer FAM-AS1411-N_3 (5'-FAM-GGT-GGT-GGT-GGT-TGT-GGT-GGT-GGT-GGT-TTT-TTT-TTT-N_3-3') (61.0 µg, 5.0 nmol, M = 12 202.1 g.mol^{-1}, 1 eq.) was solubilized in 9.7 µL of sterile aqueous buffer (pH 7.4 PBS with 1M NaCl). Then, the polymer PAF647-DBCO (580.0 µg, 50.0 nmol, M_n = 11 300 g.mol^{-1}, 10 eq.) was solubilized in 9.7 µL DMSO and then added to the first solution. The blue solution was stirred in a thermomixer (800 rpm) at 37°C for 120h. The raw product was characterized by gel electrophoresis in native conditions.

Biological evaluations.

Polyacrylamide Gel electrophoresis (PAGE). Conjugations were analyzed by polyacrylamide gel electrophoresis (PAGE, 10% acrylamide/bis-acrylamide (37.5/1) gel) in native conditions. The quantity of raw sample loaded into the gel corresponded to 1 µg of aptamer. Migration was performed at room temperature on a BioRad apparatus at 150 V in Tris-acetate (25mM), EDTA (0.5 mM) at pH 8.3 (TAE 0.5X) for 2 hours. Gels were revealed on a fluorescence imager (ChemiDoc MP, BioRad) in the far-red (λ_{ex} = 625-660 nm, λ_{em}= 675-725 nm) and the green (λ_{ex} = 460-490 nm, λ_{em}= 518-546 nm) channels. Conjugation yields were determined from PAGE gels revealed in the green channel (FAM fluorescence of the aptamer), as the free fluorescent polymer in excess is interfering in the far-red channel (Figure S8). Each band corresponding respectively

to the polymer-aptamer conjugate and free aptamer were then integrated using the densitometry tool of the ImageLab software (Figure S5). Yields were calculated from Equation 1, with $I_{free\ aptamer}$ and $I_{conjugate}$ the integrals of the free aptamer and polymer-aptamer bands, respectively.

$$Yield\ (\%) = \frac{I_{conjugate}}{I_{conjugate} + I_{free\ aptamer}} * 100 \qquad \text{Equation (1)}$$

In vitro evaluation with purified nucleolin by dot-blot analysis. Recombinant NCL-P40 protein representing the central 4 nucleic acid binding domains of nucleolin was produced as previously reported[40] by cloning the corresponding PCR fragment in the pet-15b expression vector that allows the fusion of a histidine tag at the *N*-terminus of NCL-P40 (corresponding to the construct R1234)[40]. Recombinant protein was purified from BL21(DE3)plysS transformed with pET15b-NCL-P40 plasmid. Cells grown at 37 °C in LB (100 $mg.mL^{-1}$ ampicillin, 20 $mg.mL^{-1}$ chloramphenicol, and 1 $mg.mL^{-1}$ methicillin) were induced with 1 mM isopropyl-1-thio-β-d-galactopyranoside for 4 h. Recombinant protein was purified on Ni^{2+}-nitrilotriacetic acid resin (QIAGEN) thanks to the histidine tag. After elution, the NCL-P40 protein was placed in 100 mM KCl and 10 mM Tris-HCl, pH 7.5. Concentrations were estimated with Bradford reagent (Bio-Rad protein assay) and checked by SDS-polyacrylamide gel electrophoresis.

A PVDF membrane (GE Healthcare, Amersham Hybond) was washed by immersion in 100 % ethanol during 5min, then 2×5min in water and finally 5min in PBS 1X. 0.6 µg of proteins (NCL-P40,[40] Bovine Serum Albumin-BSA or Streptavidin- SA) were spotted on the membrane. The complete adsorption of the proteins on the membrane was performed at 4°C overnight, then the membrane was washed in PBS 1X during 2h at room temperature, then 3×20 min with PBS 1X, 0.05% Tween and finally 3×10min in PBS 1X. The membrane was then incubated with a polymer-

aptamer probe solution (130 nM in PBS 1X, raw Conjugate **G** in Table S3) for 2h at room temperature in the dark. The membrane was finally washed 3×10min in PBS-T. The membrane was revealed on a fluorescence imager (ChemiDoc MP, BioRad) in the far-red (λ_{ex} = 625-660 nm, λ_{em}= 675-725 nm) and the green (λ_{ex} = 460-490 nm, λ_{em}= 518-546 nm) channels.

***In cellulo* evaluation of PAF647-AS1411-FAM probe by fluorescence microscopy.**

Incubation on live cells for cell-surface nucleolin labeling. hTERT-RPE1 cells (ATCC, CRL 4000) were grown at 37 °C in a 5% CO_2 incubator in Dulbecco's modified Eagle medium/F12 without phenol red (ThermoFisher, ref 21041025), supplemented with 10% inactivated fetal bovine serum (PAA ref: A15-101 Gold.), 1% penicillin/streptomycin solution (ThermoFisher, ref :15140-122) and 1% non-essential amino-acids (ThermoFisher, ref 11140035). 40 000 RPE1 cells were plated in regular medium as previously described[1] onto clean and sterile glass coverslips (diameter 18 mm, thickness 170 ± 5 µm, quality 1.5 H, Marienfeld Superior, Ref 0117580). After 12h, medium was replaced by SVF depleted medium to allow for cell differentiation during 60h. Three days after plating, live cells were incubated for 1h30 at 4°C with raw PAF647-AS1411-FAM probe (Conjugate **G** in Table S3) or controls (PAF647-DBCO, PAF647-Crich-FAM (Conjugate **7** in Table 2)) diluted at 0.1 µM aptamer in Opti-MEM (Gibco, 31985-062). A washing step with Opti-MEM was performed at RT to remove unbound probes. Cells were then submitted to a 10 min fixation with PFA (paraformaldehyde, 4% in 1X PBS, pH 7.2, Fluka 76240). A quenching step with 100mM Tris pH 7.2 was performed for 5min, followed by a 2x 5min permeabilization step with PBS-T (1X PBS with 0.1% Triton X-100). An indirect immunofluorescence procedure was then applied to detect endogenous NCL. After a 45min

blocking step at 37°C in blocking buffer (BB, BSA 3%, 10% SVF, PBS-T, 0.02% NaN_3), the first antibody was incubated for 45min at 37°C (NCL 4E2- Lifescience KAM-CP100- diluted at 1/150 in BB). After 2x 10min washing steps at RT on a moving table in PBS-T, the secondary antibody (Donkey anti-mouse-DL550- Agrisera AS121937, diluted at 1:250 in BB) was incubated for 45min at 37°C, followed by washing steps as before. Dried coverslips were mounted onto glass slides for microscopy observation after a PBS wash, rinse in ddH_2O and brief dipping in absolute ethanol with Fluoromount G (FMG Southern biotech Ref 0100-01) containing 400 $ng.mL^{-1}$ *4',6'*-diamidino-*2*-phenylindole (DAPI). As previously described,[41] multi-color Z-stacks (0.2 µm step size) were acquired with Zen Blue software using a Cool Snap HQ charge coupled-device camera mounted on a Zeiss Axio-Imager Z1 equipped with a 63x oil-immersion objective lens (numerical aperture [NA]=1.4 / working distance 0.19 mm) and fluorescence filters suited for DAPI, AlexaFluor 488, DL-550 and AlexaFluor 647 visualization. Displayed images correspond to an expanded depth of focus projection of about 5 selected sections in-focus for cell surface, visualized as an individual colored channel or merged channels (Figures 7 and S12).

Incubation on fixed/permeabilized cells for nucleolar labeling. 100 000 hTERT-RPE1 cells were plated as previously and fixed after 24 hours in SVF supplemented medium. A 1X-PBS/ 0.05% TX-100 solution was applied for 45sec at RT to allow pre-extraction of soluble proteins. Fixation was performed for 5 min on ice with pure cold methanol, followed by 2x 5min permeabilization step with PBS-T. Raw PAF647-AS1411-FAM probe (Conjugate **G** in Table S3) or controls (PAF647-DBCO, AS1411-FAM) were diluted at 0.1 µM in blocking buffer (BB) with anti-NCL primary antibody (4E2, diluted 1/150 in BB) and incubated for 45min at 37°C onto fixed cells. After 2x 10min washing steps at RT on a moving table in PBS-T, the secondary detection was performed either with a Donkey-anti-mouse-DL550 or with a Goat anti-mouse-AF488

(ThermoFisher A-11029, diluted at 1:1000 in BB) or with an anti-mouse-AF647 (Invitrogen A21237, diluted at 1/100 in BB). Coverslips were washed, mounted and imaged as described in the previous section (Figure S12).

PAF647-AS1411-FAM probe vs. a fluorescently-labeled primary antibody for cell surface nucleolin labeling. C3H10T (ATCC, CCL-226) cells were grown in MEM 1X without phenol red (ThermoFisher, ref 51200046) supplemented with 1% L-glu (ThermoFisher, ref 25030024), 10% inactivated fetal bovine serum (PAA ref A15-101 Gold.) and 1% penicillin/streptomycin solution (ThermoFisher, ref 15140122) and 1% non-essential amino-acids (Thermo Fisher, ref 11140035). 33 000 cells were plated onto polylysine-coated IBIDI glass 35mm dishes (high glass bottom, ref 81158) and grown for 96h. Cell surface nucleolin labeling was performed by incubation onto live cells for 1h30 at 4°C either with raw PAF647-AS1411-FAM probe (Conjugate **G** in Table S3), diluted at 0.1 µM aptamer in Opti-MEM) or with a fluorescent rabbit anti-NCL-ATTO488 primary antibody (Sigma N6288, diluted at 1/300 in Opti-MEM). After a washing step, cells were then fixed for 10 min with Formol-Zn (Formol 1.85% containing 154 mM NaCl and 10.5 mM Zn Sulfate). Coverslips were washed, mounted and imaged as described in previous sections (Figure 8).

dSTORM super-resolution nanoscopy. C3H10T cells were incubated with PAF647-AS1411-FAM probe as described above. After formol-zinc fixation and a 5min quenching step in 100mM Tris pH 7.2, dishes were rinsed in PBS and quickly mounted with 450 µl of Everspark buffer (Idylle Labs) on a 25 mm glass coverslip sealed with the twinsil dental paste as previously described.[42] dSTORM acquisitions were performed on an ELYRA 7 imaging system using the Zen Black software (Zeiss). Samples were observed with an alpha Plan-Apochromatic 63X/1.46 oil Corr M27 TIRF (#420780-9970-000) objective using a 1.6x magnification lens. A full-size image

in brightfield and fluorescence was acquired with an EMCCD camera (Andor iXon 897 Ultra, pixel size: 16 µm, 512 × 512). Pumping step was achieved for less than 30 s in HILO illumination mode (52°) with ultra-high power using 10% of the 642 nm laser (500 mW nominal power), with the corresponding LP 655 filter position. Acquisition of 20 000 images using a ROI centered around the structure was achieved with a 7% laser power with the following camera parameters: 120 for EM-gain (max value at 300) at 33 Hz rate. Z-stabilization was achieved with the Definite Focus system (Zeiss) activated during all the acquisition procedure (with piezo). Data analysis was carried out with the Zen Black software (Zeiss) as follows: (i) gaussian fitting: peak mask size = 9 pix and peak intensity to noise = 6 (ignore overlap mode). Image sampling was set to ½ of the measured localization precision (i.e. 5 or 10 nm) in a given size ROI surrounding the structure.; (ii) drift correction: using the "model-based" set up at a maximum of 30 segments, based on an auto-correlation method; (iii) connection: grouping of events using 5 frames for the maximum "ON" time, 10 frames for off gap and 1 pixel for capture radius. Displayed images on Figure 9 correspond to the probe at the cell surface visualized in epifluorescence mode as a large field of view and a zoomed region, and the reconstructed dSTORM image of the same region**.**

RESULTS AND DISCUSSION

Synthesis of ω-chain-end functionalized fluorescent polymer chains. Two types of fluorescent polymer probes bearing a reactive chain-end were synthesized to promote an oriented conjugation with AS1411 aptamer, first by amidation using the well-known activated ester/amine coupling, and second by strain-promoted azide-alkyne click chemistry (SPAAC) introduced more recently by Bertozzi *et al.*.[38] The chain-end was functionalized in the first case with a *N*-hydroxysuccinimide activated ester (NHS Ester), and in the second with a dibenzylcyclooctyne (DBCO) reactive group. In addition to chain-end functionalization, several AF647 fluorophores were covalently bound in lateral position of the chains (named PAF647). AF647 fluorophore was chosen because it is one of the most efficient photo-switchable dye for dSTORM super-resolution imaging.[14] Furthermore, this negatively charged water-soluble cyanine derivative is emitting in the far-red, a wavelength range where penetration depth of light into biological tissue is increased and auto-fluorescence is limited, compared to the rest of the visible spectrum.

Synthesis of the fluorescent polymer was based on our modular platform produced by RAFT copolymerization of *N*-acryloylmorpholine (NAM) with *N*-acryloxysuccinimide (NAS), exhibiting a controlled M_n and low dispersity ($Đ < 1.1$). At the azeotropic composition (60 mol% NAM, 40 mol% NAS), microstructure of the Poly(NAM-*stat*-NAS) precursor chains is efficiently controlled.[39] NAM units provide water-solubility and biocompatibility, while NAS units, regularly distributed along the backbone and bearing activated ester units, provide handles for the efficient coupling of a controlled number of amino-functionalized fluorescent organic dyes. Capping of the residual NAS units with aminoethylmorpholine (AEM) finally leads to water-soluble fluorescent

polymer chains and at the same time induces the aminolysis of the dithiobenzoate ω-chain-end into a thiol (PAF647-SH chains, Figure 2).

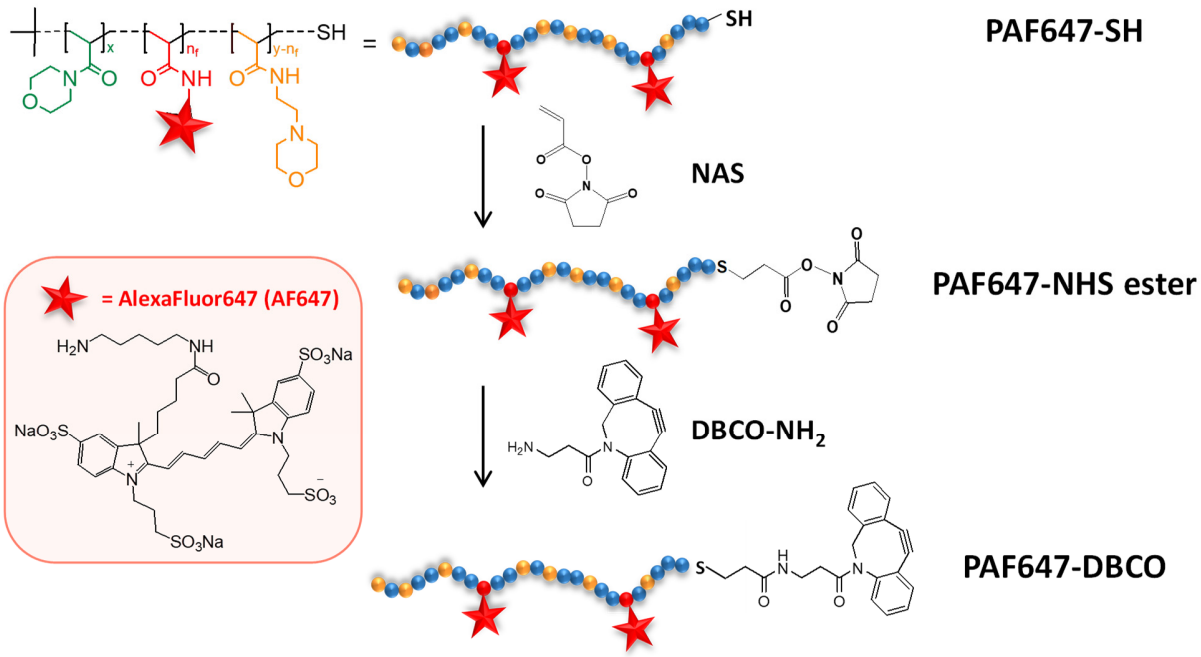

Figure 2. Representation of the ω-end functionalization with a DBCO reacting group of a hydrophilic copolymer chain labeled with AlexaFluor647 dyes (PAF647-DBCO).

Additional introduction of a reactive group at the fluorescent polymer chain-end is not trivial however we have already demonstrated that the thiol ω-chain-end can react quantitatively with NAS, to yield fluorescent polymer chains with a ω-NHS Ester chain-end able to label native proteins.[22] The same chain-end functionalization and characterization protocol was used here to obtained PAF647 chains with a NHS Ester end-group (PAF647-NHS ester). For the synthesis of PAF647 chains bearing a DBCO end-group (PAF647-DBCO), functionalization had to be

performed post-polymerization since radical polymerization can induce the degradation of the DBCO cyclooctyne. Considering our versatile synthetic protocol of fluorescent polymer chains, it was introduced after fluorophore coupling. PAF647-NHS ester chains were reacted with the amino-derivative DBCO-NH_2 (Figure 2), preventing potential thiol-yne reaction between thiol-terminated polymer chains and the DBCO group. We already showed by both NMR and MALDI-TOF-MS that this coupling strategy was very efficient and quantitative for the synthesis of low molecular weight PNAM homopolymers bearing a DBCO ω-chain-end.[43]

Thanks to our approach, molecular weight and number of fluorophores per chain can be tuned. For this proof of concept study, polymer chains with a M_n <10 000 g.mol^{-1} and bearing 2 AF647 fluorophores per chain were synthesized to facilitate chain-end characterization by NMR. A P(NAM-*stat*-NAS) copolymer precursor was prepared by RAFT polymerization in optimized conditions (M_n = 8 900 g.mol^{-1}, $Đ$ = 1.1, with 34.4 NAM units and 22.7 NAS units per chain on average). Because of the solubility profile of AF647, fluorophore coupling was then performed in DMF. As determined by SEC-UV (Figure S3), an average of 2.0 AF647 was covalently bound in lateral position of the polymer backbone to lead to thiol-terminated fluorescent polymer chains (PAF647-SH) after AEM capping. PAF647-SH was reacted with NAS to obtain PAF647-NHS ester, and then subsequently with DBCO-NH_2 to obtain PAF647-DBCO. For sake of comparison, the same DBCO chain-end functionalization was conducted with ≈10 000 g.mol^{-1} reference homo- (PNAM) and co-polymer (CPAEM) devoid of AF647 fluorophores (Table 1). In these cases, conversely to PAF647, reactions could be performed in chloroform which has already shown to be a good solvent for such functionalization.[43]

Table 1. Characteristics of the polymer samples and calculated yields determined by ^{1}H NMR

Sample	M_n (g.mol^{-1})	N_f[a]	Solubility	^{1}H NMR analyses	
				Solvent	Calculated yield (%)[b]
PNAM-DBCO	10 600	0	$CHCl_3$, H_2O, DMF	$CDCl_3$	90
				D_2O	60
CPAEM-DBCO	9 300	0	$CHCl_3$, H_2O, DMF	$CDCl_3$	100
				D_2O	30
PAF647-DBCO	11 300	2.0	H_2O, DMF	DMF-d_7	50
				D_2O	n.a.

[a] average number of fluorescent dyes per polymer chain determined by SEC-UV at 647 nm

[b] Determined by comparing the integral value of the ω-DBCO signal at 5.1ppm (1H) and the α-^{t}Bu signal (9H) at 0.8ppm.

Characterization of DBCO ω-chain-end functionalized polymer. Characterization of the chain-ends of such fluorescent polymer chains is particularly challenging. Chain-ends represent only a low proportion of the whole polymer chain (less than 1% of the total M_n) and thus could hardly be analyzed separately. For PAF647, characteristic UV absorption of the DBCO between 250-300 nm overlaps with the tail of the large one corresponding to the amide bounds of the polymer backbone (<250 nm) and with a secondary absorption band of AF647 fluorophores (Figure S6). Moreover, MALDI-TOF-MS analyses cannot give precise chain-end information for such terpolymers due to the large number of generated peaks that leads to a poor signal-to-noise ratio. Here, ^{1}H NMR was used. The same PAF647-DBCO sample was characterized in both DMF-d_7 and D_2O. In DMF-d_7, in addition to the polymer backbone and AF647 fluorophore signals, new large signals characteristic of the DBCO ω-chain-end appeared in the aromatic region (7.0 - 8.0

ppm) and at 5.1 ppm (Figure 3A). In this case, a functionalization yield of 50 ±10 % was estimated by comparing the integrals of the α-^{t}Bu (0.9 ppm, 9H, noted 1) and ω-DBCO (5.1ppm, 1H, noted 41) signals. Conversely, when the same sample was analyzed in D_2O, no such DBCO signals were detected (Figure S7).

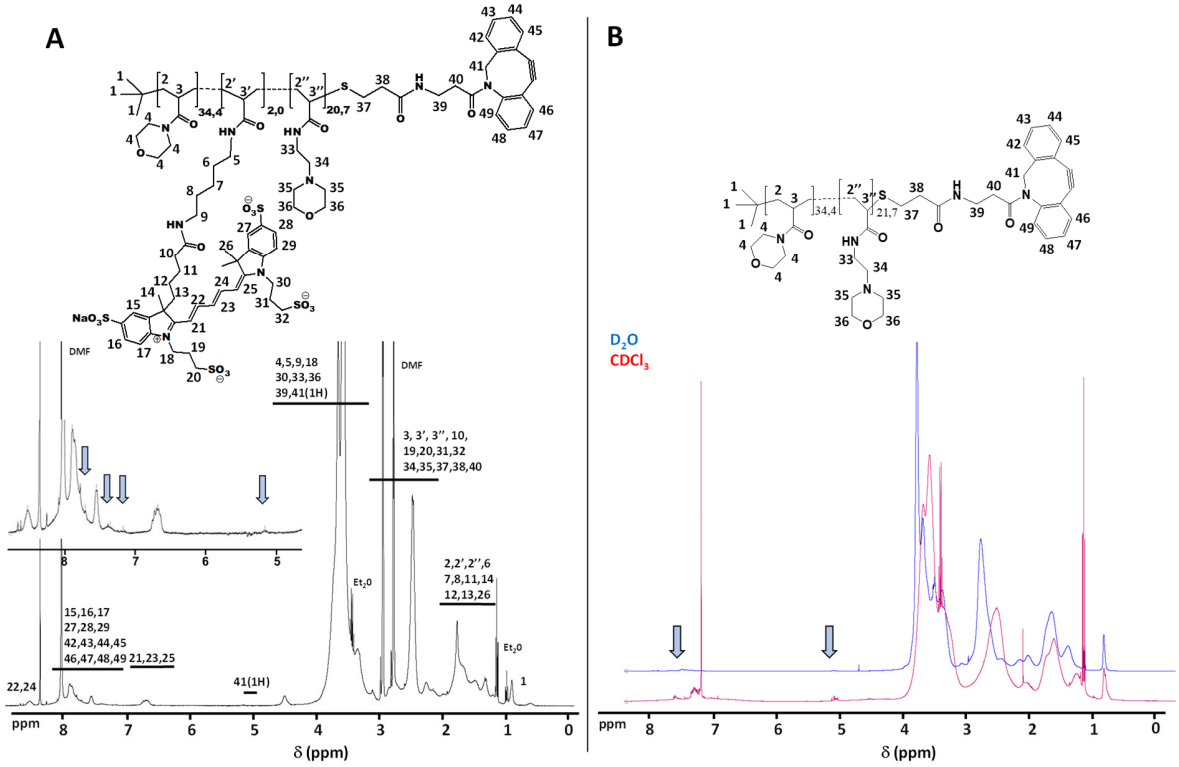

Figure 3. ^{1}H NMR spectra of polymers after purification. A) PAF647-DBCO in DMF-d_7 (DP_n = 57, M_n = 11 300 g.mol^{-1}). B) CPAEM-DBCO reference copolymer without AF647 fluorophores (DP_n = 57, M_n = 9 300 g.mol^{-1}) in D_2O (blue) and $CDCl_3$ (red). Arrows indicates characteristic DBCO signals.

To understand these discrepancies between DMF-d_7 and D_2O analyses of PAF647-DBCO, the reference polymer chains without AF647 were also characterized by ^{1}H NMR in $CDCl_3$ (Figure 3B, red spectrum) and then in D_2O (Figure 3B, blue spectrum). For both PNAM and CPAEM

polymers, DBCO chain-end signals were clearly observed in $CDCl_3$ and their intensity was much lower in D_2O. The functionalization yield determined by the above-mentioned method was almost quantitative in $CDCl_3$ whereas it dropped significantly in D_2O (by 40 to 70%, Table 1). The most drastic difference was observed for the CPAEM copolymer for which the calculated yield was 100% in $CDCl_3$ and only 30% in D_2O.

In conclusion, while DBCO functionalization is effective, precise yield determination was hampered by the influence of solvent on NMR analyses. Synthesis and characterization were facilitated with chloroform as solvent. NMR analyses however showed that the DBCO signals were much less visible in D_2O. It probably reflects that the hydrophobic DBCO end-groups are not well solvated in polar solvents. From these results, it appears probable that the functionalization yield determined in DMF-d_7 for PAF647-DBCO is underestimated. Nevertheless, further confirmation of the presence of the DBCO group at the chain-end of PAF647-DBCO chains could arise from their conjugation with azido-modified AS1411 aptamer.

Conjugation of ω-chain-end functionalized PAF647 fluorescent polymer chains with AS1411 aptamer. PAF647 fluorescent polymer chains were then conjugated to AS1411 aptamer in an oriented manner via their respective chain-ends. This conjugation strategy and the presence of a spacer between the aptamer and the chain should indeed favor the G-quadruplex folding of AS1411 aptamer and limit the effect of steric hindrance on nucleolin recognition. As mentioned above, two types of PAF647-AS1411 conjugation were considered (Figure 4): First, by amidation between PAF647-NHS ester and an aptamer functionalized with a primary amine (Aptamer-NH_2). Second by SPAAC between PAF647-DBCO and an aptamer functionalized with an azide group (Aptamer-N_3), that has the advantage of avoiding the use of potentially toxic catalysts. Concerning

the aptamer, the 3'-end was modified in each case with a 10-thymine spacer (T_{10}) before introduction of the reactive end-group (amine or azide), while the 5'-end was labeled with a fluorescein-based dye (FAM, $\lambda_{ex\ max}$ = 494 nm and $\lambda_{em\ max}$ = 514 nm) for sake of characterization.

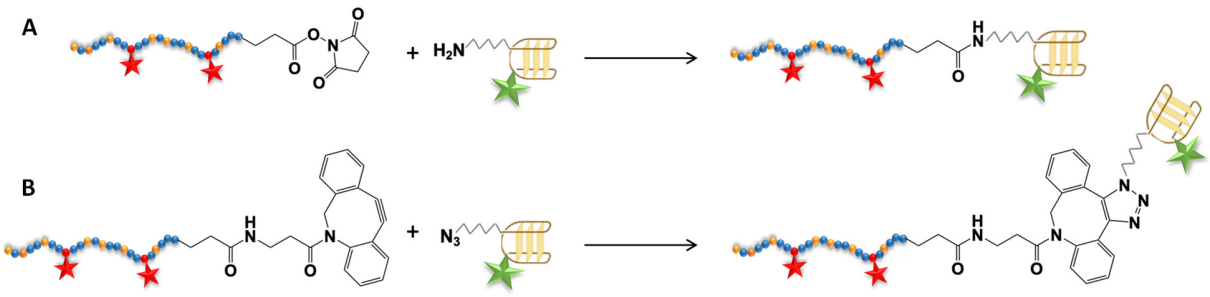

Figure 4. Polymer-aptamer conjugation strategies A) by amidation between ω-NHS ester polymer chain and amino-functionalized aptamer B) by SPAAC between ω-DBCO polymer chain and azido-functionalized aptamer.

For both conjugation strategies, various experimental parameters such as the solvent composition and ionic strength were varied to optimize polymer-aptamer conjugation (See Supporting Information). Ionic strength of the aqueous buffer was increased to reduce the electrostatic repulsion between PAF647 and aptamer that are both negatively charged macromolecules. In addition, DMSO was added in different proportion to the aqueous buffer[26] to favor the accessibility of the activated ester and DBCO polymer chain-ends. Finally, conjugation assays were also performed with CPAEM-reference polymer that does not bear AF647 fluorophores and negative charges.

Conjugation by amidation between PAF647-NHS ester and FAM-AS1411-NH_2 aptamer was investigated in comparison to a similar conjugation of the same aptamer with small NHS-ester AF647 molecular dye (AF647-NHS ester) (Table S2 and Figure S8). Whereas aptamer conjugation yield was high with the AF647-NHS ester molecular dye (75%), it was much lower with PAF647-NHS ester polymer (<5%). This difference in yield reflected a slow kinetics of the PAF647-NHS ester conjugation that can be notably ascribed to the multiple electrostatic repulsions with AS1411 and a reduced accessibility of NHS-ester groups at the polymer chain-end compared to the small dye. The concomitant hydrolysis of the NHS ester reactive group which is in competition with conjugation thus probably become preponderant in this situation. This hypothesis was further confirmed by a complementary conjugation assay with CPAEM-NHS ester reference polymer that does not bear negatively charged AF647 fluorophores (Table S2 and Figure S9). In this case, polymer-aptamer conjugation yield was much higher (71%), confirming the significant impact of electrostatic repulsion. These results were in striking contrast with those obtained when PAF647-NHS ester was shown to efficiently react with the lysine amines of proteins (streptavidin, lysozyme) that are less densely charged.[22]

Table 2. Conjugation between DBCO ω-chain-end polymers and azide functionalized aptamers.

Conjugate	Aptamer-N_3	Polymer[a]	Polymer/aptamer molar ratio	Solvent (PBS pH7.4 : DMSO) vol%[c]	Duration (h)	Yield[b] (%)
1	FAM-AS1411-N_3	CPAEM-DBCO	10	(50:50)	72	60
2		PAF647-DBCO	10	(20:80)	120	27
3			3	(50:50)	3	3
4			10	(50:50)	72	19
5			10	(50:50)	120	36
6	FAM-AS1411-PEG-N_3		10	(50:50)	120	50
7	FAM-Crich-N_3		10	(20:80)	120	16

[a] Polymer concentration was 30 $mg.mL^{-1}$

[b] Yield estimated using ImageLab software (Figure S5)

Then, polymer-aptamer conjugation was evaluated by SPAAC with ω-DBCO polymers (Table 2). First, two conjugations of the fluorescent aptamer FAM-AS1411-N_3 with CPAEM-DBCO (Conjugate **1**) and PAF647-DBCO (Conjugate **4**) polymers were compared (Figure 5A).

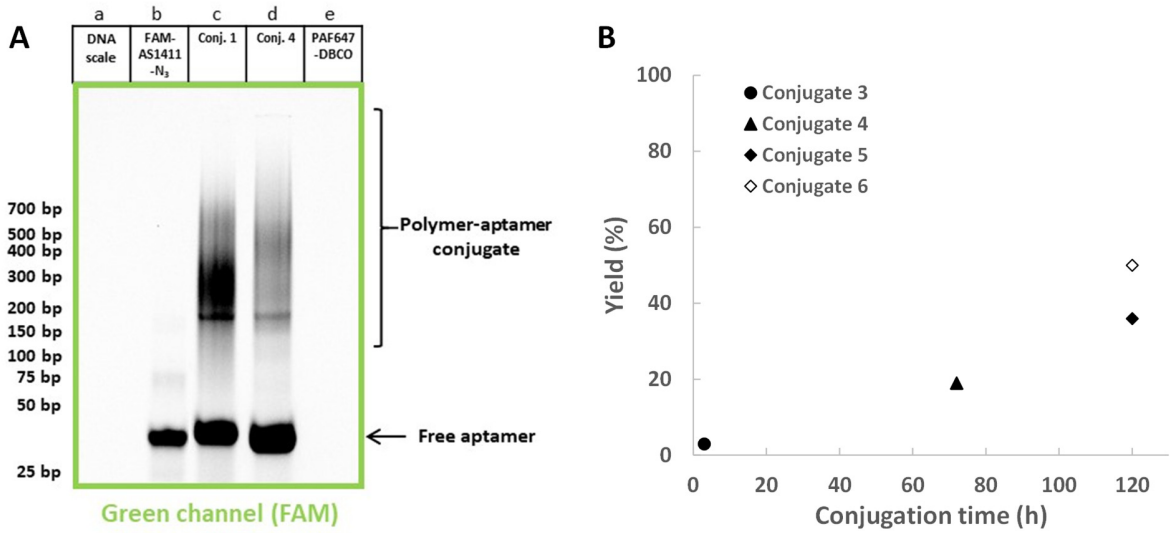

Figure 5. SPAAC polymer-aptamer conjugation. A) Characterization by native gel electrophoresis with revelation in the green channel (FAM fluorescence). a – Non-fluorescent DNA Scale, b – FAM-AS1411-N_3 free aptamer, c - Conjugate **1** (FAM-AS1411-N_3 + CPAEM-DBCO), d – Conjugate **4** (FAM-AS1411-N_3 + PAF647-DBCO), e – PAF647-DBCO free polymer. The indicative DNA ladder given on the left was obtained from the revelation of the same gel under UV irradiation (B) Yield vs. time of conjugation between PAF647-DBCO and azido-functionalized AS1411 aptamers for different assays without (full labels) and with (open label, Conjugate **6**) an additional PEG spacer between the azide function and the aptamer.

For both reactions, a large smear characteristic of polymer-aptamer conjugate formation was observed above the free fluorescent aptamer band. Compared to amidation, SPAAC conjugation between PAF647-DBCO fluorescent polymer and FAM-AS1411-N_3 was more efficient (Conjugate **4**; 19% yield). Conjugation yield was again higher with the CPAEM reference

copolymer without AF647 fluorophore (Conjugate **1**, 60%), confirming that the absence of negative charges on the polymer favors conjugation.

To further improve conjugation between PAF647-DBCO and FAM-AS1411-N_3 aptamer, several experimental conditions were varied (Table S3 and Figure S10). Only solvent composition and especially conjugation time appeared to have a significant impact (Table 2). Conjugation yield slightly decreased when DMSO proportion in the solvent was increased from 50 to 80 vol% (*e.g.* Conjugate **5** vs. Conjugate **2** respectively), probably due to a lower solvation of the aptamer. In addition, yield more significantly increased with conjugation duration (Figure 5B). Conversely to amidation, reactive end-groups are less subjected to degradation during SPAAC conjugation. Finally, an additional PEG spacer was added between aptamer 3'-T_{10} sequence and the azide reactive end-group. PEG being non-charged, more flexible and well soluble in the solvent mixture, it could provide more accessibility to the azide end-group for reaction with the ω-DBCO end-group of the polymer. The presence of this extra spacer seemed to be beneficial since a 50% conjugation yield was obtained (Conjugate **6**).

Finally, various conjugates were successfully obtained by SPAAC coupling that clearly showed to be more advantageous than amidation in this context. A conjugation was notably performed with PAF647-DBCO and another nucleotide sequence FAM-Crich-N_3 (Conjugate **7**, 16%), that is similar to FAM-AS1411-N_3 aptamer but with cytosines (C) replacing guanines (G). The latter thus do not adopt a G-quadruplex conformation and do not selectively recognize nucleolin. PAF647-Crich-FAM conjugate can then be used as a negative control for the biological evaluations of PAF647-AS1411-FAM aptamer conjugates.

***In vitro* evaluation of the nucleolin selective recognition by the polymer-aptamer conjugate.**

The ability of the PAF647-AS1411 polymer-aptamer conjugate to recognize nucleolin (NCL) was first evaluated *in vitro* by dot-blot analysis. A purified nucleolin sub-domain (NCL-P40, 40 kDa) that carries the binding domain to AS1411 aptamer[14,15] was blotted on a PVDF membrane alongside bovine serum albumin (BSA, 66 kDa) and streptavidin (SA, 55 kDa), both used as negative controls. The membrane was then incubated with a solution of the raw PAF647-AS1411-FAM polymer-aptamer conjugate (130 nM), before fluorescence detection in the green (FAM) and the far-red (AF647) channels (Figure 6).

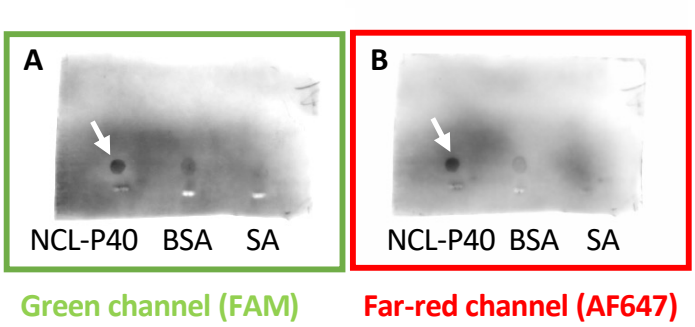

Figure 6. Dot-blot experiment revealed (A) in the green channel (FAM fluorophore, λ_{exc}=488 nm) and (B) in the far-red channel (AF647 fluorophore, λ_{exc}=647nm). 0.6 µg of three native proteins were deposited on the PVDF membrane. From left to right: NCL-P40 (nucleolin sub-unit carrying its AS1411 binding domain), bovine albumin serum (BSA) and streptavidin (SA). The membrane was then incubated with a PBS solution of raw PAF647-AS1411-FAM polymer-aptamer conjugate (130 nM).

Such analysis revealed that NCL-P40 dot was strongly labeled by the polymer-aptamer probe whereas the non-specific signal from the BSA and SA dots significantly faded after the washing

steps. It thus constituted a first indication that the polymer-aptamer probe was able to selectively recognize purified nucleolin.

***In cellulo* evaluation of nucleolin recognition by fluorescence microscopy.** The ability of the PAF647-AS1411 polymer-aptamer conjugate to specifically recognize native nucleolin was further evaluated *in cellulo* by fluorescence microscopy. Two different strategies, corresponding to two distinct protocols, were investigated. PAF647-AS1411-FAM was incubated either on fixed and permeabilized cells or on live cells (Figure S11, top and bottom respectively). In both cases, cell labeling was compared to the one obtained by standard immunofluorescence performed after fixation/permeabilization of the cells. This standard immunofluorescence, classically used to selectively label nucleolin, consists in an indirect two-step procedure involving in step 1 the recognition of nucleolin by a highly specific primary anti-nucleolin mouse antibody (4E2 antibody, first step), and then in step 2 the labeling of 4E2 with a fluorescent secondary anti-mouse antibody (coupled here with Dylight 550 (DL550) emitting in the red channel, distinct from FAM and AF647 emission).

When PAF647-AS1411-FAM was incubated on fixed and permeabilized cells (Figure S12, lanes A and B), far-red fluorescence from PAF647 exclusively co-localized with the green fluorescence of FAM-AS1411 aptamer, thus confirming their efficient SPAAC conjugation. Importantly, PAF647-AS1411-FAM also strongly co-localized with 4E2-mediated immunofluorescence (A.4 and B.4 panels). In these fixed and permeabilized cell conditions, the latter predominantly labels the nucleoli inside cell nucleus that represent the major pools of nucleolin inside the cell.[1] Those results thus not only confirmed that PAF647-AS1411-FAM probe recognized nucleolin, but they

also showed that, interestingly, the polymer-aptamer probe was able to access the cell nucleus. Control experiments indicated that PAF647-DBCO alone did not induce any non-specific cell labeling in the same conditions (Lane C). In addition, free AS1411-FAM aptamer gave equivalent cell labeling profile in the green channel than PAF647-AS1411-FAM (Lane D).

Incubating live cells with PAF647-AS1411-FAM probe was particularly evaluated to label nucleolin present at the cell surface (1h30, 4°C, Figure 7 and S12). We chose RPE-1 cell model based on a previous publication demonstrating the presence of cell surface nucleolin in various retinal cell types including RPE cells[44] and on preliminary studies on RPE-1 differentiated cells (KM, unpublished results). A comparison was made with indirect immunofluorescence performed after cell fixation and permeabilization, as described above. Moreover, experiments with PAF647-AS1411-FAM were compared to those conducted in the same conditions with PAF647-Crich-FAM and free PAF647-DBCO controls.

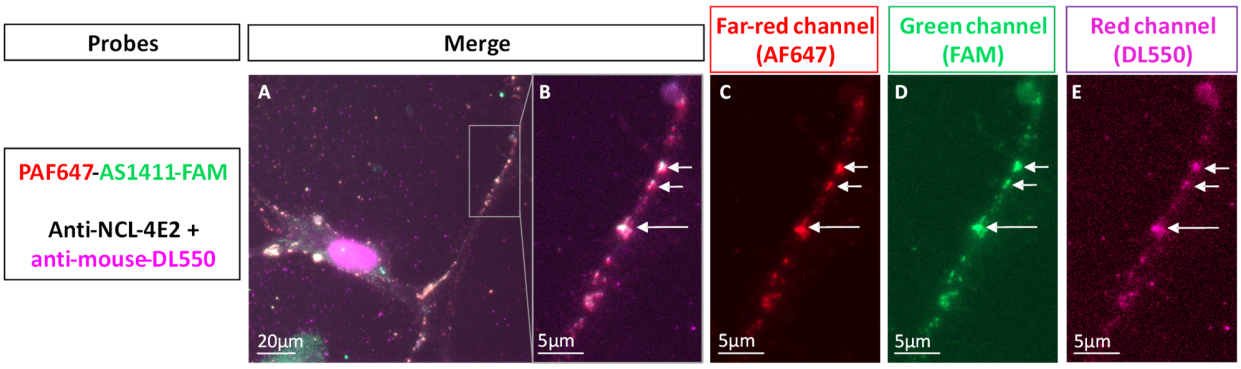

Figure 7. Cell labeling after incubation of PAF647-AS1411-FAM probe on live RPE-1 cells. For comparison, indirect immunofluorescence against NCL was performed on the same cells, but after

cell fixation. DL550 fluorescently labeled secondary antibodies were detected in the red channel (shown in purple). From the full image of a RPE1 cell (A), a region-of-interest (ROI, grey box) was selected on a cell extension. The zoom focusing on this ROI (B) merges the images showing localization of PAF647 (C, far-red channel), AS1411-FAM (D, green channel) and immunofluorescence (E, shown in purple, red channel). White arrows illustrate co-localizations. Scale: 20µm for full cell images and 5µm for zooms.

As illustrated by the points indicated by white arrows in Figure 7, strong co-localizations were witnessed at the cell surface in the far-red (PAF647), green (FAM) and red (immunofluorescence) channels. In addition, when similar experiments were performed with the free PAF647-DBCO and PAF647-Crich-FAM controls no cell labeling was observed (Figure S13). It confirmed our previous observations showing that PAF647 polymers are not permeant to live cells and do not induced non-specific cell labeling.[24]

Consequently, altogether our results further confirmed polymer-aptamer conjugation (PAF647 and FAM co-localization), showed that recognition of nucleolin by PAF647 requires conjugation with AS1411 aptamer, and demonstrated the specificity of endogenous nucleolin labeling (co-localization with immunofluorescence). In addition, it indicated that imaging can be performed without purification of the conjugate which greatly simplifies the workflow.

PAF647-AS1411 as alternative probe to fluorescent primary antibody for the labeling of cell surface nucleolin. Thanks to their physico-chemical and photo-physical properties as well as

their specific recognition for nucleolin, such polymer-aptamer probes represent very promising tools for *in vitro*, *in cellulo* and *in vivo* applications. For instance, they could provide an advantageous alternative to immunofluorescence which is widely used. Indeed, the experimental protocol is simplified and polymer-aptamer probes like PAF647-AS1411-FAM are both bright and small (<10nm).

To illustrate that point, we thus compared in parallel PAF647-AS1411-FAM probe to a fluorescent primary antibody against nucleolin (anti-NCL-ATTO488) known to efficiently label cell surface nucleolin (KM, unpublished data). Experiments were carried out on C3H10T cancer cell line, since cancer cells are known to highly express nucleolin. Conversely to the previously shown experiments, both probe incubation and immunofluorescence were performed on live C3H10T cell conditions, without preliminary fixation and permeabilization. It is noteworthy that in these live cell conditions, the indirect primary/fluorescent secondary antibody strategy (see above) would be ineffective. This is why fluorescent primary antibodies are directly used, although they are generally more prone to denaturation upon fluorescent labeling and thus exhibit a lower brightness than fluorescent secondary antibodies.

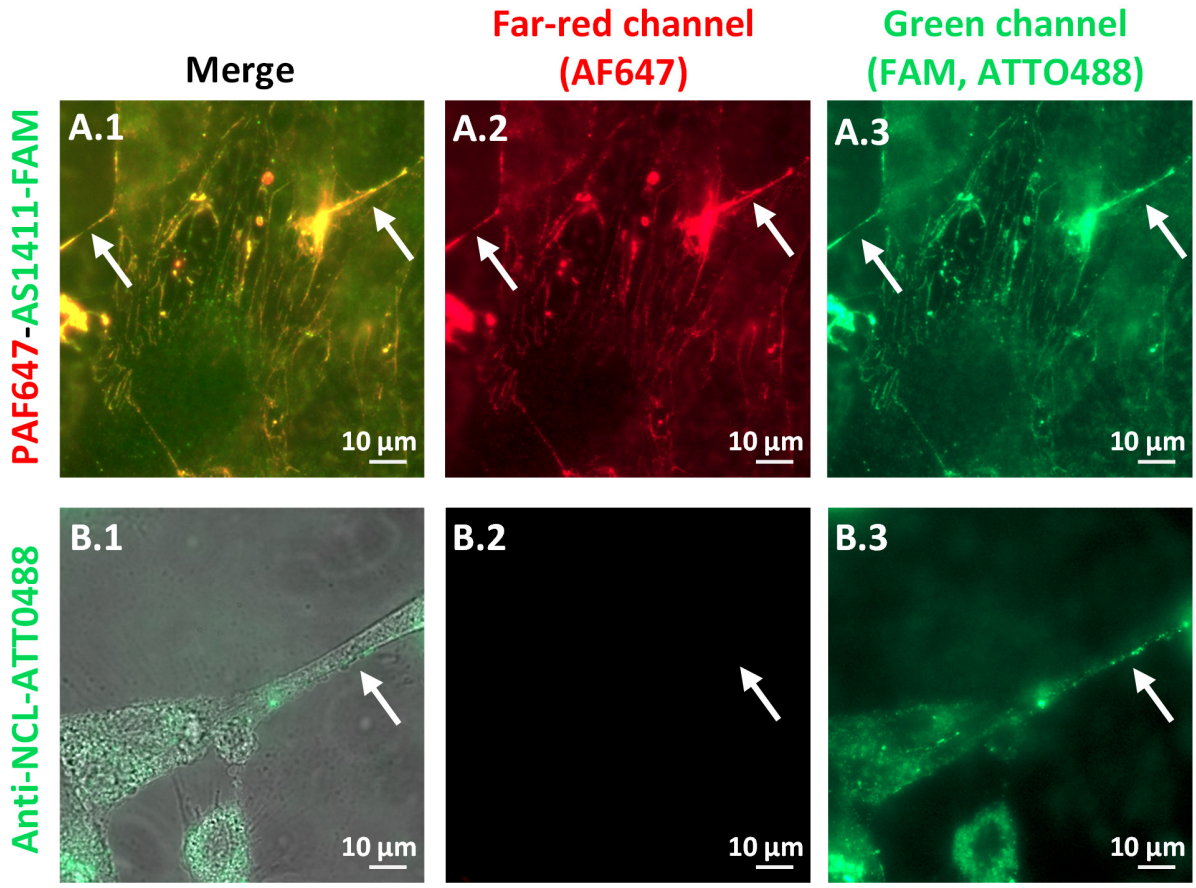

Figure 8. PAF647-AS1411-FAM localization after incubation on live cells. C3H10T cells were incubated with PAF647-AS1411-FAM probe (A) or a fluorescently-labeled primary antibody, Anti-NCL-Atto488 (B) for 1h30 at 4°C before formol Zn fixation. Bright Field was added on B.1 to better see cellular extensions. White arrows show localizations on extension. Scale: 10µm

As FAM and ATTO488 fluorophores are both detected in the same green fluorescence channel, microscopy comparison between PAF647-AS1411-FAM and anti-NCL-ATTO488 was realized in parallel on two separate slides (Figure 8). Both the polymer-aptamer probe PAF647-AS1411-FAM (Figure 8.A) and anti-NCL-ATTO488 primary antibody (Figure 8.B) were able to label

endogenous nucleolin present at the cell surface. As previously shown with RPE-1 cells, this was more clearly observed on cell membrane extensions (see white arrows in Figure 8 for examples). Nevertheless, PAF647-AS1411-FAM gave a more intense and continuous labeling compared to the fluorescent primary antibody for which more seldom events were detected. This can be ascribed to a lower labeling efficiency of the primary antibody.

Under these live cell conditions, the polymer-aptamer probe is thus more adapted and more potent than the best available immunofluorescence strategy to detect cell-surface nucleolin. Our probe therefore constitutes a very useful tools to study the role and fate of cell surface nucleolin.

dSTORM super-resolution imaging. Finally, considering the performance of PAF647-AS1411-FAM probe, it was thus important to confirm that it can be imaged by dSTORM super-resolution nanoscopy to further improve the localization precision of cell-surface nucleolin. Thanks to its small size (<10 nm) and the advantageous photo-physical properties of AF647, PAF647-AS1411 is particularly attractive for dSTORM that can achieve localization precision down to 10-20 nm. In a recent article, we have indeed proven that PAF647-lipid polymer probes grafted onto LipoParticles were able to be imaged by dSTORM with average localization precision of single fluorescence events of about 20nm. It then enabled the precise reconstruction of 1µm LipoParticles that thus represent very interesting calibration tools for such technique.[42]

PAF647-AS1411-FAM probe was tested on the C3H10T cancer cell model as described before. After an optimized fixation with Formol-Zinc, cells were first imaged in epifluorescence (Figure 9.A.1). The labeling was similar to previous observations with RPE-1 cells. A region of interest (ROI) on a cell extension that was strongly labeled by the polymer-aptamer probe (Panel A.1,

white square) was then defined and zoomed on (Panel A.1'). dSTORM imaging was performed on this ROI (Figure 9.B) by detecting AF647 blinking in a specific buffer (eternity buffer) that provides more stable and long-term imaging.[42]

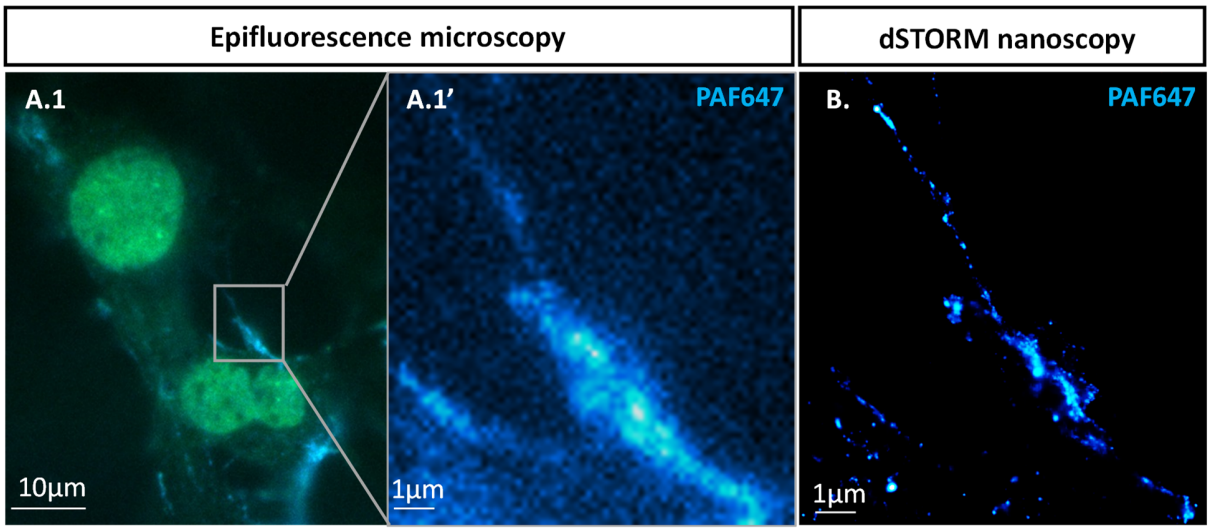

Figure 9. dSTORM imaging with PAF647-AS1411-FAM on cell extension. C3H10T cells were incubated with PAF647-AS1411-FAM probe for 1h30 at 4°C before formol-Zn fixation. (A.1) Epifluorescence image of cells merging the green (FAM) and the far-red (PAF647) channels, Scale: 10µm. (A.1') Zoom on cell membrane (grey box from A.1) in the far-red channel (PAF647). (B) Super resolution dSTORM image of A.1', 20 000 images acquisition in the far-red channel and reconstruction with Gaussian fitting leading to a much-improved resolution than epifluorescence. Zoom scale: 1µm

During acquisition, AF647 blinking was observed in the far-red channel with a high contrast. Each fluorescent event was then recorded with high localization precision (23 nm on average) and

20 000 images were taken to finally reconstruct the final image (Figure 9.B).[42] Labeling density offered by the polymer-aptamer probe led to an unprecedented image resolution and precision of localization of native nucleolin at the cell surface.

In addition, such dSTORM observations were repeated with other cell line (RPE-1 cells) and microscope set-up (Figure S14 and Movie S1). Two-color super-resolved dSTORM images with PAF647-AS1411-FAM probe were notably acquired, further confirming co-distribution of PAF647 (far-red channel) and AS1411-FAM (green channel), notably along cell extensions. It is noteworthy that acquiring such green/far-red two color dSTORM images is quite exceptional at this time.

This type of fluorescent polymer-aptamer probe is thus efficiently visualized in dSTORM conditions. It thus provides very valuable and potent tools to better understand the roles and functions of cell surface nucleolin and to explore more finely its trafficking inside cells after internalization.

CONCLUSION

Fluorescent polymer chains bearing a controlled number of dSTORM fluorophores (AlexaFluor647) were prepared by RAFT polymerization. A reactive group was then introduced at their ω-chain-end to promote their oriented conjugation with AS1411, a 26-bases DNA aptamer exhibiting a G-quadruplex conformation that binds with a high affinity nucleolin, a multifunctional protein involved in essential biological processes. Polymer-aptamer conjugation was performed through two different coupling approaches, activated ester/amine (amidation) and strained

alkyne/azide click chemistry (SPAAC). SPAAC conjugation between dibenzylcyclooctyne (DBCO)-ended fluorescent polymer chains and 3'-azido-functionalized nucleic acids proved to be the most efficient approach. *In vitro* and *in cellulo* evaluations demonstrated that the fluorescent polymer-aptamer probes were able to selectively recognize native nucleolin. Their brightness and small size make these polymer-aptamer probes an advantageous alternative to immunofluorescence, notably in the context of super-resolution fluorescence imaging. PAF647-AS1411-FAM fluorescent polymer-aptamer probe could indeed be imaged by dSTORM nanoscopy to precisely detect endogenous nucleolin present at the cell surface. This work thus paves the way toward a better understanding about the localization and functions of this protein. For instance, labeling of cell surface nucleolin is of particular interest to follow the trafficking of the aptamer-NCL complex that get rapidly internalized inside the cell upon formation.[9, 45] Only seldom information is available on this process and fluorescence super-resolution nanoscopy has the potential to unravel important insights.

ASSOCIATED CONTENT

Supporting Information. Additional experimental data, polymer characterizations, polymer-aptamer conjugations, *in cellulo* evaluations of PAF647-AS1411-FAM probe, as well as dSTORM images and movie.

AUTHOR INFORMATION

Corresponding Author

* arnaud.favier@univ-lyon1.fr

Present Addresses

† Univ Lyon 1, CNRS UMR 5310 - INSERM U1217, Institut NeuroMyoGene, Lyon, F-69008, France

Author Contributions

The manuscript was written through contributions of all authors. All authors have given approval to the final version of the manuscript.

Funding Sources

CNRS Mission pour les Initiatives Transverses et Interdisciplinaires (MITI, Imag'In Program, LENNONN project to KM). CNRS pre-maturation program (Green dSTORM project to KM)

Notes

KM and AF participated to the development of the Everspark dSTORM buffer used in this study that is provided by Idylle Labs.

ACKNOWLEDGMENT

We acknowledge Agnès Crépet (Laboratoire d'Ingénierie des Matériaux Polymères, Lyon) for technical support in SEC/MALLS measurements, Carlos Fernandez-de Alba (Laboratoire d'Ingénierie des Matériaux Polymères, Lyon) for technical support in NMR analyses. This work benefited from the facilities and expertise of the Liquid Chromatography and NMR Platforms of Institut de Chimie de Lyon, ICL (FR5223) for polymer characterization. The authors also acknowledge the contribution of PLATIM imaging facility platform (SFR Biosciences Gerland-Lyon Sud, CNRS UMS3444, INSERM US8) and in particular Elodie Chatre for technical assistance. We also thank Christophe Place (Laboratoire de Physique, ENS de Lyon) for fruitful discussions about dSTORM imaging, Idylle Labs for providing the Everspark buffer, GDR IMABIO and MiFoBio Imaging School as well as Bruker for the use of the Vutara VXL system. This work was supported by CNRS Mission pour les Initiatives Transverses et Interdisciplinaires (MITI, Imag'In program, LENNONN project). L.F. acknowledges a Ph.D. grant from the French Ministry of Research and Education.

REFERENCES

1. Berger, C. M.; Gaume, X.; Bouvet, P., The roles of nucleolin subcellular localization in cancer. *Biochimie* **2015,** *113*, 78-85.
2. Mongelard, F.; Bouvet, P., Nucleolin: a multiFACeTed protein. *Trends Cell Biol.* **2007,** *17* (2), 80-6.
3. Storck, S.; Shukla, M.; Dimitrov, S.; Bouvet, P., Functions of the histone chaperone nucleolin in diseases. *Subcell. Biochem.* **2007,** *41*, 125-44.
4. Srivastava, M.; Pollard, H. B., Molecular dissection of nucleolin's role in growth and cell proliferation: new insights. *Faseb J.* **1999,** *13* (14), 1911-22.
5. Tuteja, R.; Tuteja, N., Nucleolin: a multifunctional major nucleolar phosphoprotein. *Crit. Rev. Biochem. Mol. Biol.* **1998,** *33* (6), 407-36.
6. Abdelmohsen, K.; Gorospe, M., RNA-binding protein nucleolin in disease. *RNA Biology* **2012,** *9* (6), 799-808.
7. Mongelard, F.; Bouvet, P., AS-1411, a guanosine-rich oligonucleotide aptamer targeting nucleolin for the potential treatment of cancer, including acute myeloid leukemia. *Curr. Opin. Mol. Ther.* **2010,** *12*, 107-114.
8. Larrucea, S.; González-Rubio, C.; Cambronero, R.; Ballou, B.; Bonay, P.; López-Granados, E.; Bouvet, P.; Fontán, G.; Fresno, M.; López-Trascasa, M., Cellular Adhesion Mediated by Factor J, a Complement Inhibitor: evidence for nucleolin involvment. *J. Biol. Chem.* **1998,** *273* (48), 31718-31725.
9. Bates, P. J.; Reyes-Reyes, E. M.; Malik, M. T.; Murphy, E. M.; O'Toole, M. G.; Trent, J. O., G-quadruplex oligonucleotide AS1411 as a cancer-targeting agent: Uses and mechanisms. *Biochim. Biophys. Acta (BBA) - General Subjects* **2017,** *1861* (5, Part B), 1414-1428.
10. Shi, H.; Huang, Y.; Zhou, H.; Song, X.; Yuan, S.; Fu, Y.; Luo, Y., Nucleolin is a receptor that mediates antiangiogenic and antitumor activity of endostatin. *Blood* **2007,** *110* (8), 2899-2906.
11. Gilles, M.-E.; Maione, F.; Cossutta, M.; Carpentier, G.; Caruana, L.; Di Maria, S.; Houppe, C.; Destouches, D.; Shchors, K.; Prochasson, C.; Mongelard, F.; Lamba, S.; Bardelli, A.; Bouvet, P.; Couvelard, A.; Courty, J.; Giraudo, E.; Cascone, I., Nucleolin Targeting Impairs the Progression of Pancreatic Cancer and Promotes the Normalization of Tumor Vasculature. *Cancer Res.* **2016,** *76* (24), 7181.
12. Perrone, R.; Butovskaya, E.; Lago, S.; Garzino-Demo, A.; Pannecouque, C.; Palù, G.; Richter, S. N., The G-quadruplex-forming aptamer AS1411 potently inhibits HIV-1 attachment to the host cell. *Int. J. Antimicrobial agents* **2016,** *47* (4), 311-6.
13. Schermelleh, L.; Ferrand, A.; Huser, T.; Eggeling, C.; Sauer, M.; Biehlmaier, O.; Drummen, G. P. C., Super-resolution microscopy demystified. *Nat. Cell Biol.* **2019,** *21* (1), 72-84.
14. Karlsson, J. K. G.; Laude, A.; Hall, M. J.; Harriman, A., Photo-isomerization of the Cyanine Dye Alexa-Fluor 647 (AF-647) in the Context of dSTORM Super-Resolution Microscopy. *Chemistry – A Eur. J.* **2019,** *25* (65), 14983-14998.
15. Heilemann, M.; van de Linde, S.; Mukherjee, A.; Sauer, M., Super-Resolution Imaging with Small Organic Fluorophores. *Angew. Chem. Int. Ed.* **2009,** *48* (37), 6903-6908.
16. Soundararajan, S.; Wang, L.; Sridharan, V.; Chen, W.; Courtenay-Luck, N.; Jones, D.; Spicer, E. K.; Fernandes, D. J., Plasma Membrane Nucleolin Is a Receptor for the Anticancer Aptamer AS1411 in MV4-11 Leukemia Cells. *Mol. Pharm.* **2009,** *76* (5), 984-991.

17. Sharma, V. R.; Thomas, S. D.; Miller, D. M.; Rezzoug, F., Nucleolin Overexpression Confers Increased Sensitivity to the Anti-Nucleolin Aptamer, AS1411. *Cancer Invest.* **2018,** *36* (9-10), 475-491.
18. Soundararajan, S.; Chen, W.; Spicer, E. K.; Courtenay-Luck, N.; Fernandes, D. J., The Nucleolin Targeting Aptamer AS1411 Destabilizes BCL-2 Messenger RNA in Human Breast Cancer Cells. *Cancer Res.* **2008,** *68* (7), 2358.
19. Yazdian-Robati, R.; Bayat, P.; Oroojalian, F.; Zargari, M.; Ramezani, M.; Taghdisi, S. M.; Abnous, K., Therapeutic applications of AS1411 aptamer, an update review. *Int. J. Biol. Macromolecules* **2020,** *155*, 1420-1431.
20. Cepraga, C.; Gallavardin, T.; Marotte, S.; Lanoe, P.-H.; Mulatier, J.-C.; Lerouge, F.; Parola, S.; Lindgren, M.; Baldeck, P. L.; Marvel, J.; Maury, O.; Monnereau, C.; Favier, A.; Andraud, C.; Leverrier, Y.; Charreyre, M.-T., Biocompatible Well-Defined Chromophore-Polymer Conjugates for Photodynamic Therapy and Two-Photon Imaging. *Polym. Chem.* **2013,** *4*, 61-67.
21. Adjili, S.; Favier, A.; Fargier, G.; Thomas, A.; Massin, J.; Monier, K.; Favard, C.; Vanbelle, C.; Bruneau, S.; Peyriéras, N.; Andraud, C.; Muriaux, D.; Charreyre, M.-T., Biocompatible photoresistant far-red emitting, fluorescent polymer probes, with near-infrared two-photon absorption, for living cell and zebrafish embryo imaging. *Biomaterials* **2015,** *46*, 70-81.
22. Duret, D.; Haftek-Terreau, Z.; Carretier, M.; Berki, T.; Ladavière, C.; Monier, K.; Bouvet, P.; Marvel, J.; Leverrier, Y.; Charreyre, M. T.; Favier, A., Labeling of native proteins with fluorescent RAFT polymer probes: application to the detection of a cell surface protein using flow cytometry. *Polym. Chem.* **2018,** *9* (14), 1857-1868.
23. Duret, D.; Haftek-Terreau, Z.; Carretier, M.; Ladaviere, C.; Charreyre, M.-T.; Favier, A., Fluorescent RAFT polymers bearing a nitrilotriacetic acid (NTA) ligand at the α-chain-end for the site-specific labeling of histidine-tagged proteins. *Polym. Chem.* **2017**, *8*, 1611-1615.
24. Berki, T.; Bakunts, A.; Duret, D.; Fabre, L.; Ladavière, C.; Orsi, A.; Charreyre, M.-T.; Raimondi, A.; van Anken, E.; Favier, A., Advanced Fluorescent Polymer Probes for the Site-Specific Labeling of Proteins in Live Cells Using the HaloTag Technology. *ACS Omega* **2019,** *4* (7), 12841-12847.
25. Chamignon, C.; Duret, D.; Charreyre, M.-T.; Favier, A., 1H DOSY NMR Determination of the Molecular Weight and the Solution Properties of Poly(N-acryloylmorpholine) in Various Solvents. *Macromol. Chem. and Phys.* **2016,** *217* (20), 2286-2293.
26. Ladaviere, C.; Delair, T.; Domard, A.; Pichot, C.; Mandrand, B., Covalent immobilization of biological molecules to maleic anhydride and methyl vinyl ether copolymers—A physico-chemical approach. *J. Appl. Polym. Sci.* **1999,** *71* (6), 927-936.
27. de Lambert, B.; Chaix, C.; Charreyre, M.-T.; Laurent, A.; Aigoui, A.; Perrin-Rubens, A.; Pichot, C., Polymer-Oligonucleotide Conjugate Synthesis from an Amphiphilic Block Copolymer. Applications to DNA Detection on Microarray. *Bioconjugate Chem.* **2005,** *16* (2), 265-274.
28. Minard-Basquin, C.; Chaix, C.; Pichot, C.; Mandrand, B., Oligonucleotide−Polymer Conjugates: Effect of the Method of Synthesis on Their Structure and Performance in Diagnostic Assays. *Bioconjugate Chem.* **2000,** *11* (6), 795-804.
29. Alemdaroglu, F. E.; Herrmann, A., DNA meets synthetic polymers—highly versatile hybrid materials. *Org. Biomol. Chem.* **2007,** *5* (9), 1311-1320.
30. Oishi, M.; Sasaki, S.; Nagasaki, Y.; Kataoka, K., pH-Responsive Oligodeoxynucleotide (ODN)−Poly(Ethylene Glycol) Conjugate through Acid-Labile β-Thiopropionate Linkage: Preparation and Polyion Complex Micelle Formation. *Biomacromolecules* **2003,** *4* (5), 1426-1432.

31. Wilks, T. R.; O'Reilly, R. K., Efficient DNA–Polymer Coupling in Organic Solvents: A Survey of Amide Coupling, Thiol-Ene and Tetrazine–Norbornene Chemistries Applied to Conjugation of Poly(N-Isopropylacrylamide). *Sci. Rep.* **2016,** *6* (1), 39192.
32. Costioli, M. D.; Fisch, I.; Garret-Flaudy, F.; Hilbrig, F.; Freitag, R., DNA purification by triple-helix affinity precipitation. *Biotechnol.Bioeng.* **2003,** *81* (5), 535-545.
33. Da Pieve, C.; Williams, P.; Haddleton, D. M.; Palmer, R. M. J.; Missailidis, S., Modification of Thiol Functionalized Aptamers by Conjugation of Synthetic Polymers. *Bioconjugate Chem.* **2010,** *21* (1), 169-174.
34. Healy, J. M.; Lewis, S. D.; Kurz, M.; Boomer, R. M.; Thompson, K. M.; Wilson, C.; McCauley, T. G., Pharmacokinetics and Biodistribution of Novel Aptamer Compositions. *Pharm.l Res.* **2004,** *21* (12), 2234-2246.
35. Deng, Z.; Yang, Q.; Peng, Y.; He, J.; Xu, S.; Wang, D.; Peng, T.; Wang, R.; Wang, X.-Q.; Tan, W., Polymeric Engineering of Aptamer–Drug Conjugates for Targeted Cancer Therapy. *Bioconjugate Chem.* **2020,** *31* (1), 37-42.
36. Oh, S. S.; Lee, B. F.; Leibfarth, F. A.; Eisenstein, M.; Robb, M. J.; Lynd, N. A.; Hawker, C. J.; Soh, H. T., Synthetic Aptamer-Polymer Hybrid Constructs for Programmed Drug Delivery into Specific Target Cells. *J. Am. Chem. Soc.* **2014,** *136* (42), 15010-15015.
37. Wilks, T. R.; Bath, J.; de Vries, J. W.; Raymond, J. E.; Herrmann, A.; Turberfield, A. J.; O'Reilly, R. K., "Giant Surfactants" Created by the Fast and Efficient Functionalization of a DNA Tetrahedron with a Temperature-Responsive Polymer. *ACS Nano* **2013,** *7* (10), 8561-8572.
38. Agard, N. J.; Prescher, J. A.; Bertozzi, C. R., A Strain-Promoted [3 + 2] Azide−Alkyne Cycloaddition for Covalent Modification of Biomolecules in Living Systems. *J. Am. Chem. Soc.* **2004,** *126* (46), 15046-15047.
39. Favier, A.; D'Agosto, F.; Charreyre, M. T.; Pichot, C., Synthesis of N-acryloxysuccinimide copolymers by RAFT polymerization, as reactive building blocks with full control of composition and molecular weights. *Polymer* **2004,** *45* (23), 7821-7830.
40. Serin, G.; Joseph, G.; Ghisolfi, L.; Bauzan, M.; Erard, M.; Amalric, F.; Bouvet, P., Two RNA-binding Domains Determine the RNA-binding Specificity of Nucleolin. *J. Biol. Chem.* **1997,** *272* (20), 13109-13116.
41. Gaume, X.; Tassin, A.-M.; Ugrinova, I.; Mongelard, F.; Monier, K.; Bouvet, P., Centrosomal nucleolin is required for microtubule network organization. *Cell Cycle* **2015,** *14* (6), 902-919.
42. Provost, A.; Rousset, C.; Bourdon, L.; Mezhoud, S.; Reungoat, E.; Fourneaux, C.; Bresson, T.; Pauly, M.; Béard, N.; Possi-Tchouanlong, L.; Grigorov, B.; Bouvet, P.; Diaz, J.-J.; Chamot, C.; Pécheur, E.-I.; Ladavière, C.; Charreyre, M.-T.; Favier, A.; Place, C.; Monier, K., Innovative particle standards and long-lived imaging for 2D and 3D dSTORM. *Sci. Rep.* **2019,** *9* (1), 17967.
43. Favier, A.; Duret, D.; Charreyre, M. T. Process for the preparation of a polymer by sequence addition of monomers. French Patent FR3020634A1, 2014.
44. Leaderer, D.; Cashman, S. M.; Kumar-Singh, R., G-quartet oligonucleotide mediated delivery of proteins into photoreceptors and retinal pigment epithelium via intravitreal injection. *Experim. Eye Res.* **2016,** *145*, 380-392.
45. Fogal, V.; Sugahara, K. N.; Ruoslahti, E.; Christian, S., Cell surface nucleolin antagonist causes endothelial cell apoptosis and normalization of tumor vasculature. *Angiogenesis* **2009,** *12* (1), 91-100.

For Table of Contents Use Only.

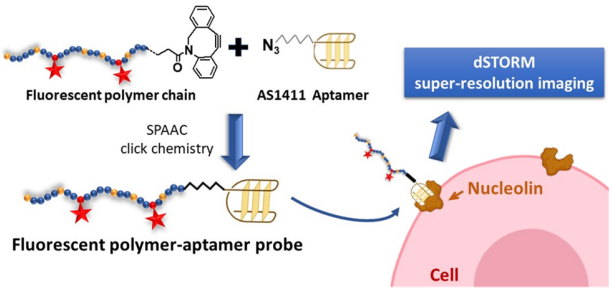

Fluorescent polymer-AS1411-aptamer probe for dSTORM super-resolution imaging of endogenous nucleolin

Laura Fabre,[1] Corentin Rousset,[2†] Karine Monier,[2†] Fernande Da Cruz-Boisson,[1] Philippe Bouvet,[2] Marie-Thérèse Charreyre,[1] Thierry Delair,[1] Etienne Fleury,[1] Arnaud Favier[1]*